ChemPubSoc Europe

DOI: 10.1002/open.201500208

Open Access ChemistryOPEN Full Papers

Alkali Metal Cation versus Proton and Methyl Cation Affinities: Structure and Bonding Mechanism

Zakaria Boughlala,[a] Célia Fonseca Guerra,[a] and F. Matthias Bickelhaupt*[a, b]

We have analyzed the structure and bonding of gas-phase Cl–X and $[HCl–X]^+$ complexes for $X^+ = H^+$, CH_3^+, Li^+, and Na^+, using relativistic density functional theory (DFT). We wish to establish a quantitative trend in affinities of the anionic and neutral Lewis bases Cl^- and HCl for the various cations. The Cl–X bond becomes longer and weaker along $X^+ = H^+$, CH_3^+, Li^+, and Na^+. Our main purpose is to understand the heterolytic bonding mechanism behind the intrinsic (i.e., in the absence of solvent) alkali metal cation affinities (AMCA) and how this compares with and differs from those of the proton affinity (PA) and methyl cation affinity (MCA). Our analyses are based on Kohn–Sham molecular orbital (KS-MO) theory in combination with a quantitative energy decomposition analysis (EDA) that pinpoints the importance of the different features in the bonding mechanism. Orbital overlap appears to play an important role in determining the trend in cation affinities.

1. Introduction

Designing and optimizing routes in chemical synthesis requires knowledge of the thermochemistry involved in the targeted compounds or reactions. The alkali metal cation affinity (AMCA) is a thermochemical quantity that plays an important role for predicting and understanding stability as well as reactivity in structures and processes in which such ions bind to, and/or dissociate from Lewis-basic nitrogen, oxygen, and other atoms. Examples are lithium and sodium battery electrochemistry,[1] alkali metal cation transport in biological systems (e.g., sodium or potassium cations in ion channels in cell membranes),[2,3] stabilization of nucleic acid structures (DNA, RNA and PNA),[4] and the dissociation of salts.[5,6] However, the ACMA has received relatively little attention in the literature and if compared with, for example, the proton affinity (PA).[7]

The thermochemical quantity ACMA is defined as the enthalpy change associated with heterolytic dissociation of the complex between the alkali metal cation (X^+) and the anionic (B^-) or neutral base (B):

$$BX \rightarrow B^- + X^+ \quad \Delta H = \mathrm{AMCA} \tag{1}$$

$$BX^+ \rightarrow B + X^+ \quad \Delta H = \mathrm{AMCA} \tag{2}$$

The purpose of the present study is twofold. The main objective is to obtain a better understanding of the physical factors behind the AMCA. To this end, we have carried out a detailed analysis of the bonding mechanism behind the intrinsic (i.e., in the absence of interfering solvent effects) ACMA of a negative and a neutral model base, namely, chloride and hydrogen chloride, for both the lithium and the sodium cation ($B^- = Cl^-$, $B = HCl$, $X^+ = Li^+$, Na^+ in [Equations (1)–(2)]. Our analysis has been carried out in the conceptual framework of Kohn–Sham molecular orbital (KS-MO) theory in combination with a quantitative energy decomposition analyses (EDA).

In the second place, we wish to compare the nature of ACMA with that of the corresponding PA[7a,b,c] and methyl cation affinities (MCA).[8] Thus, $X^+ = H^+$ and CH_3^+ are included in our discussion of the bonding mechanism. In addition to the ACMA values of all bases (ΔH^{298}_{AMCA}), we also report the corresponding 298 K reaction entropies (ΔS^{298}_{AMCA}, provided as $-T\ \Delta S^{298}_{AMCA}$) and 298 K reaction Gibbs-free energies (ΔG^{298}_{AMCA}).

2. Computational Methods

2.1. Basis sets

All calculations were performed with the Amsterdam Density functional (ADF) program developed by Baerends and others.[9,10] Molecular orbitals (MOs) were expanded using two large, uncontracted sets of Slater-type orbitals (STO): TZ2P for geometry optimization and vibrational analysis, and QZ4P for single-point energy calculations.[11] The TZ2P basis set is of triple-ζ quality, augmented by two sets of polarization functions (*d* and *f* on heavy atoms; 2*p* and 3*d* sets on H). The QZ4P

[a] Z. Boughlala, Dr. C. Fonseca Guerra, Prof. Dr. F. M. Bickelhaupt
Department of Theoretical Chemistry
and Amsterdam Center for Multiscale Modeling (ACMM)
VU University Amsterdam, De Boelelaan 1083
1081 HV Amsterdam (The Netherlands)
E-mail: F.M.Bickelhaupt@vu.nl

[b] Prof. Dr. F. M. Bickelhaupt
Institute of Molecules and Materials
Radboud University Nijmegen, Heyendaalseweg 135
6525 AJ Nijmegen (The Netherlands)

Supporting information and the ORCID identification number(s) for the author(s) of this article can be found under http://dx.doi.org/10.1002/open.201500208.

basis, which contains additional diffuse functions, is of quadruple-ζ quality, augmented by four sets of polarization functions (two 3*d* and two 4*f* sets on C, N, O; two 2*p* and two 3*d* sets on H). Core electrons (e.g., 1*s* for second-period, 1*s*2*s*2*p* for third-period, 1*s*2*s*2*p*3*s*3*p* for fourth-period, 1*s*2*s*2*p*3*s*3*p*3*d*4*s*4*p* for fifth-period, and 1*s*2*s*2*p*3*s*3*p*3*d*4*s*4*p*4*d* for sixth-period atoms) were treated by the frozen core approximation.[10] An auxiliary set of *s*, *p*, *d*, *f*, and *g* slater-type orbitals was used to fit the molecular density and to represent the coulomb and exchange potentials accurately in each self-consistent field (SCF) cycle.

2.2. Density functional

Energies and gradients were calculated using the local density approximation (LDA: Slater[12] exchange and VWN[13] correlation) with gradient corrections[14,15] due to Becke (exchange) and Perdew (correlation) added self-consistently. This is the BP86 density functional, which is one of the three best DFT functionals for the accuracy of geometries[7a–b,16] with an estimated unsigned error of 0.009 Å in combination with the TZ2P basis set. In a previous study[7a–c] on the proton affinities of anionic species, we compared the energies of a range of other DFT functionals, to estimate the influence of the choice of DFT functional. These functionals included the Local Density Approximation (LDA), Generalized Gradient Approximation (GGAs), *meta*-GGA and hybrid functionals. Scalar relativistic corrections were included self-consistently using the zeroth order regular approximation (ZORA).[17] Spin-orbit coupling effects were neglected because they are small for closed-shell systems as they occur in this investigation.

Geometries, vibrational frequencies, and thermodynamic corrections have been computed using the TZ2P basis set: ZORA-BP86/TZ2P level. All electronic energies have been computed in a single-point fashion using the QZ4P basis set, based on the ZORA-BP86/TZ2P geometries: ZORA-BP86/QZ4P//ZORA-BP86/TZ2P. For comparison, we have also computed the above-mentioned quantities using the B3LYP hybrid functional[18] in combination with TZ2P basis set for the geometries and frequencies calculations, and with QZ4P for the single-point energies, that is, ZORA-B3LYP/QZ4P//ZORA-B3LYP/TZ2P. Note that bonding analyses have been carried out at the ZORA-BP86/TZ2P level of theory.

2.3. Thermochemistry

Enthalpies at 298.15 K and 1 atmosphere (ΔH_{298}) were calculated from electronic bond energies (ΔE) at ZORA-BP86/QZ4P//ZORA-BP86/TZ2P and vibrational frequencies at ZORA-BP86/TZ2P using standard thermochemistry relations for an ideal gas, according to [Eq. (3)]:[19]

$$\Delta H_{298} = \Delta E + \Delta E_{\mathrm{trans},298} + \Delta E_{\mathrm{rot},298} + \Delta E_{\mathrm{vib},0} + \Delta(\Delta E_{\mathrm{vib},0})_{298} + \Delta(pV) \quad (3)$$

Here, $\Delta E_{\mathrm{trans},298}$, $\Delta E_{\mathrm{rot},298}$ and $\Delta E_{\mathrm{vib},0}$ are the differences between the reactant (i.e., $BX^{(+)}$, the base-cation complex) and products (i.e., $B^{(-)}+X^{+}$, the neutral or anionic base and the cation) in translational, rotational and zero point vibrational energy, respectively. $\Delta(\Delta E_{\mathrm{vib},0})_{298}$ is the change in the vibrational energy difference as one goes from 0 to 298.15 K. The vibrational energy corrections are based on our frequency calculations. The molar work term $\Delta(pV)$ is $(\Delta n)RT$; $\Delta n = +1$ for one reactant BX dissociating into two products B^{-} and X^{+}. Thermal corrections for the electronic energy are neglected.

2.4. Bond-energy decomposition

As mentioned above, bonding analyses have been carried out at the ZORA-BP86/TZ2P level of theory. The overall bond energy ΔE_{bond} (which corresponds to $-\Delta E$ in [Eq. (3)]) between base $B^{(-)}$ and cation X^{+} is made up of two major components:[20]

$$\Delta E_{\mathrm{bond}} = \Delta E_{\mathrm{strain}} + \Delta E_{\mathrm{int}} \quad (4)$$

Here, the strain energy, $\Delta E_{\mathrm{strain}}$, is the amount of energy required to deform the separate base and cation from their equilibrium structure to the geometry that they acquire in the overall complex $BX^{(+)}$. The interaction energy ΔE_{int} corresponds to the actual energy change when the geometrically deformed base and cation are combined to form the overall complex.

The interaction ΔE_{int} can be further analyzed, in the framework of the Kohn–Sham molecular orbital (MO) model, using an energy decomposition into electrostatic interaction attraction, Pauli repulsion, and (attractive) orbital interactions:[9,20]

$$\Delta E_{\mathrm{int}} = \Delta V_{\mathrm{elstat}} + \Delta E_{\mathrm{Pauli}} + \Delta E_{\mathrm{oi}} \quad (5)$$

The term $\Delta V_{\mathrm{elstat}}$ corresponds to the classical electrostatic interaction between the unperturbed charge distributions of the prepared (i.e., deformed) base and cation. This term is usually attractive. The Pauli-repulsion $\Delta E_{\mathrm{Pauli}}$ comprises the destabilizing interactions between occupied orbitals and is responsible for the steric repulsion. The orbital interaction ΔE_{oi} in any MO model, and therefore also in Kohn–Sham theory, accounts for charge transfer (i.e., donor–acceptor interactions between occupied orbitals on one moiety with unoccupied orbitals of the other, including the HOMO–LUMO interactions) and polarization (empty/occupied orbital mixing on one fragment due to the presence of another fragment).

2.5. Analysis of the charge distribution

The electron density distribution is analyzed at ZORA-BP86/TZ2P using the Voronoi deformation density (VDD) method[21,22] for computing atomic charges. The VDD atomic charge $Q_{\mathrm{A}}^{\mathrm{VDD}}$ is computed as the (numerical) integral[23] of the deformation density $\Delta\rho(\mathbf{r}) = \rho(\mathbf{r}) - \Sigma_{\mathrm{B}}\ \rho_{\mathrm{B}}(\mathbf{r})$ in the volume of the Voronoi cell of atom A [Eq. (6)]. The Voronoi cell of atom A is defined as the compartment of space bound by the bond midplanes on and perpendicular to all bond axes between nucleus A and its neighboring nuclei (cf. the Wigner–Seitz cells in crystals).[22c]

$$Q_A^{VDD} = -\int_{\text{atom A}}^{\text{Voronoi cell}} \left[\rho(r) - \sum_B \rho_B(r)\right] dr \quad (6)$$

In [Eq. (6)], $\rho(\mathbf{r})$ is the electron density of the molecule and $\Sigma_B\ \rho_B(\mathbf{r})$ the superposition of atomic densities ρ_B of a fictitious promolecule without chemical interactions that is associated with the situation in which all atoms are neutral. The interpretation of the VDD charge Q_A^{VDD} is rather straightforward and transparent. Instead of measuring the amount of charge associated with a particular atom A, Q_A^{VDD} directly monitors how much charge flows, due to chemical interactions, out of ($Q_A^{VDD} > 0$) or into ($Q_A^{VDD} < 0$) the Voronoi cell of atom A, that is, the region of space that is closer to nucleus A than to any other nucleus.

3. Results and Discussion

3.1. Structures and energies

Our computed ZORA-BP86/QZ4P//BP86/TZ2P geometries and affinities at 298 K (ΔH), the corresponding entropies ΔS (provided as $-T\Delta S$ values) and free energies ΔG are summarized in Tables 1 and 2 for the chloride and hydrogen chloride bases,

Table 1. Cation affinity data (in kcal mol^{-1}, Å) for the chloride anion.

Cation	H^+	CH_3^+	Li^+	Na^+
$-T\,\Delta S$[a]	−5.4	−7.9	−5.2	−5.1
ΔG[a]	328.2	223.5	147.7	126.9
ΔH_{BP86}[a]	333.6	231.4	152.9	132.0
ΔH_{B3LYP}[b]	332.7	224.1	155.2	133.9
ΔH_{MP2}[c]	331.3	228.6	153.9	134.5
ΔH_{exp}[d]	333.5 ± 0.002	227.3 ± 0.6	152.0	132.6
d(X–Cl)[a]	1.292	1.801	2.030	2.377
d(X–Cl)$_{Exp}$[d]	1.275	1.785	2.021	2.361

[a] This work. Computed at ZORA-BP86/QZ4P//ZORA-BP86/TZ2P for 298.15 K and 1 atm. In parentheses: enthalpies computed at ZORA-BP86/TZ2P. [b] This work. Computed at ZORA-B3LYP/QZ4P//ZORA-B3LYP/TZ2P for 298.15 K and 1 atm. [c] MP2 values from Refs. [24], [25] and [26]. [d] Experimental values from Refs. [24], [27] and [28].

respectively. In both tables we compare the results for ZORA-BP86/QZ4P//BP86/TZ2P with ZORA-B3LYP/QZ4P//B3LYP/TZ2P and MP2 calculations as well as with the experiment. As expected,[7a,b] both functionals BP86 and B3LYP emerge as good functionals (vide infra), they agree for both ClX and $[HCl–X]^+$ complexes within a few hundredths of an Å (Cl–X distances) and a few kcal mol^{-1} (298 K heterolytic bonds dissociation enthalpies ΔH) with the available experimental and/or other computational reference data.[24–33] Both functionals show mean absolute deviation (MAD) values of 2.0 kcal mol^{-1} with respect to the experimental values, while MP2 achieves a slightly worse MAD value of 2.5 kcal mol^{-1}. Based on the results of previous studies[7a,b] on the proton affinities, where BP86 functional emerges slightly more accurate than B3LYP, we have chosen to continue our calculation using BP86.

Table 2. Cation affinity data (in kcal mol^{-1}, Å, degrees) for hydrogen chloride.

Cation	H^+	CH_3^+	Li^+	Na^+
$-T\,\Delta S$[a]	−5.9	−8.7	−5.4	−5.0
ΔG[a]	130.2	46.1	10.3	4.8
ΔH_{BP86}[a]	136.2	54.8	15.7	9.9
ΔH_{B3LYP}[b]	135.0	49.2	16.9	10.9
ΔH_{MP2}[c]	134.2	45.7	15.7	8.9
ΔH_{exp}[d]	133.1	51.6	n.a.	12.1 ± 1.5
d(X–Cl)[a]	1.324	1.876	2.351	2.755
d(Cl–H)[a]	1.324	1.315	1.302	1.299
(X–Cl–H)[a]	93.6	99.5	103.6	106.1

[a] This work Computed at ZORA-BP86/QZ4P//ZORA-BP86/TZ2P for 298.15 K and 1 atm. In parentheses: enthalpies computed at ZORA-BP86/TZ2P. [b] This work. Computed at ZORA-B3LYP/QZ4P//ZORA-B3LYP/TZ2P for 298.15 K and 1 atm. [c] MP2 values from Refs. [29], [30] and [31]. [d] Experimental values from Refs. [28], [32] and [33] (n.a. = not available).

In the neutral complexes ClX, between chloride and the various cations, the X–Cl bond distance increases systematically from 1.292 to 1.801 to 2.030 to 2.377 Å along $X^+ = H^+$, CH_3^+, Li^+, and Na^+, respectively (see Table 1). At the same time, the cation affinity of the chloride anion, that is, ΔH for reaction 1 (with $B^- = Cl^-$), decreases if one goes from 333.6 (H^+) to 231.4 (CH_3^+) to 152.9 (Li^+) to 132.0 kcal mol^{-1} (Na^+; see Table 1). The corresponding Gibbs free energies $\Delta_{acid}G_{298}$ show the same trends because entropy corrections $-T\Delta_{acid}\ S_{298}$ are relatively small, between −5.1 and −7.9 kcal mol^{-1}.

Likewise, in the cationic complexes $[HCl–X]^+$ between hydrogen chloride and the various cations, the X–Cl bond distance increases again systematically from 1.324 to 1.876 to 2.351 to 2.755 Å along $X^+ = H^+$, CH_3^+, Li^+ and Na^+, respectively (see Table 2). At the same time, as the X–Cl bond becomes longer, the H–Cl bond contracts, although only very slightly so (from 1.324 to 1.315 to 1.302 to 1.299 Å) and the H–Cl–X angle adopts a substantially less bent configuration (varying from 93.6° to 99.5° to 103.6° to 106.1°). The cation affinity of the hydrogen chloride molecule, that is, ΔH for reaction 2 (with B = HCl), decreases along the same series from 136.2 (H^+) to 54.8 (CH_3^+) to 15.7 (Li^+) to 9.9 kcal mol^{-1} (Na^+; see Table 2). Again, the corresponding Gibbs free energies ΔG show the same trends as ΔH.

3.2. Bonding mechanism: Cl^- cation affinities

Our heterolytic Cl–X bonding analyses have been carried out at ZORA-BP86/TZ2P and comprise three complementary approaches: 1) quantitative analysis of the Kohn–Sham orbital interaction mechanism; 2) the associated bond energy decomposition; and 3) analysis of the electron-density distribution (see Table 3 and Figure 1). The trend in cation affinity ΔH, an enthalpic quantity, is determined by that in the electronic cation affinity energy ΔE associated with reaction 1. Note that,

Table 3. Analysis of the X–Cl bonding mechanism between Cl^- and X^+.[a]

		Cation X^+			
		H^+	CH_3^+	Li^+	Na^+
Bond energy decomposition (in kcal mol^{-1})					
ΔE_σ		−157.5	−184.6	−13.6	−8.1
ΔE_π		−22.1	−21.6	−12.5	−6.9
ΔE_{oi}		−179.6	−206.2	−26.1	−14.9
ΔE_{Pauli}		0.0	156.4	30.2	26.0
ΔV_{elstat}		−159.9	−211.9	−159.6	−145.1
ΔE_{int}		−339.5	−261.6	−155.5	−134.0
ΔE_{strain}		0.0	24.7	0.0	0.0
ΔE_{bond}		−339.5	−236.9	−155.5	−134.0
$\Delta H_{bond} = -\Delta H_{TZ2P}$		−336.3	−234.4	−155.4	−134.2
X^+ Fragment orbital energy (in eV)					
ε_{LUMO}		−13.6	−15.4[b]	−6.9	−7.1
$\langle Cl^- \vert X^+ \rangle$ *Fragment orbital overlap*		$\langle 3p_\sigma \vert 1s \rangle$	$\langle 3p_\sigma \vert 2a_1 \rangle$	$\langle 3p_\sigma \vert 2s \rangle$	$\langle 3p_\sigma \vert 3s \rangle$
$\langle HOMO \vert LUMO \rangle$		0.52	0.35	0.29	0.26
Fragment orbital populations (in e)[c]					
Cl^-	$HOMO^{-1}$	1.89 (3*s*)	1.96 (3*s*)	1.96 (3*s*)	1.98 (3*s*)
	HOMO	1.27 ($3p_\sigma$)	1.22 ($3p_\sigma$)	1.82 ($3p_\sigma$)	1.84 ($3p_\sigma$)
X^+	LUMO	0.74 (1*s*)	0.81 ($2a_1$)	0.08 (2*s*)	0.12 (3*s*)
	LUMO + 1	0.02 (2*s*)[d]	0.01 ($3a_1$)	0.08 ($2p_\sigma$)	0.03 ($3p_\sigma$)
VDD atomic charges (in a.u.)					
Q(X in XCl)		+0.098	+0.131[e]	+0.475	+0.567

[a] Computed at ZORA-BP86/TZ2P. See also Methods section. [b] Orbital energy of CH_3^+ in the geometry it adopts in $ClCH_3$. [c] Pertinent orbital indicated in parentheses. [d] $P(2p_\sigma) = 0.04$ e. [e] Sum of atomic charges on CH_3 moiety.

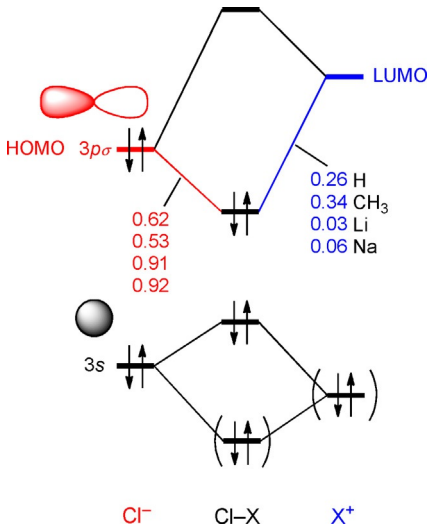

Figure 1. Orbital interaction diagram for XCl composed of Cl^- and X^+, emerging from our Kohn–Sham orbital analyses at ZORA-BP86/TZ2P ($X^+ = H^+$, CH_3^+, Li^+, Na^+). In bold: Gross Mulliken frontier molecular orbital (FMO) contributions to the molecular orbital (MO). Parentheses indicate no Pauli repulsion for $X^+ = H^+$.

for the bonding analysis, we use the bond energy $\Delta E_{bond} = -\Delta E$, that is, the energy change associated with bond formation $Cl^- + X^+ \rightarrow ClX$ (see Table 3). The main contributor to $\Delta E_{bond} = \Delta E_{strain} + \Delta E_{int}$, in turn, is the interaction energy ΔE_{int} between the two fragments which determines the overall trend in stability. ΔE_{int} weakens strongly from −339.5 to −261.6 to −155.5 to −134.0 along H^+, CH_3^+, Li^+ and Na^+. The strain energy ΔE_{strain} does not affect this trend in interaction. ΔE_{strain} is exactly zero kcal mol^{-1} for all monoatomic fragments (chloride, proton, alkali metal cations). Only in the case of the methyl cation, there is a destabilizing strain energy of 24.7 kcal mol^{-1} which originates from the fact that planar CH_3^+ must deform into a pyramidal geometry as it binds to Cl^-. This strain effect is too small to change the overall trend in relative stability ΔE_{bond}.

The trend in ΔE_{int} originates from a combination of two phenomena in the bonding mechanism (see Table 3): 1) the orbital interactions ΔE_{oi} and electrostatic attraction ΔV_{elstat} are strongest for CH_3^+ (−206.2 and −211.9 kcal mol^{-1}) and become systematically weaker as we further proceed to H^+, Li^+ and Na^+; 2) a sizeable Pauli repulsion ΔE_{Pauli} of 156.4 kcal mol^{-1} causes the methyl cation affinity (MCA) to become smaller than the proton affinity (PA). The strong Pauli repulsion in the case of CH_3^+ results from the overlap of the Cl^- 3*s* and especially $3p_\sigma$ AOs with the C–H bonding valence $1a_1$ orbital of CH_3^+.[8] Such Pauli repulsion was shown to play an even more important role in complexes between sterically more demanding bases and alkyl cations.[37,38] The chloride anion has zero Pauli repulsion with the proton (the latter has no electrons at all) and only little Pauli repulsion (26-30 kcal mol^{-1}) with the alkali metal cations which have electrons only in very compact core AOs.

The weakening in ΔE_{oi} along CH_3^+, H^+, Li^+, and Na^+ can be traced directly to covalent features in the bonding mechanism, in particular, the HOMO–LUMO interactions in the σ-electron system (see Figure 1 and Table 3). First, the energy of the cation LUMO increases drastically as we go from the methyl cation and proton (−15.4 eV and −13.6 eV) to the alkali metal cations (−6.9 and −7.1 eV). Second, the HOMO–LUMO bond overlap decreases systematically when the LUMO, as can be seen in Figure 2, contains more nodal surfaces and becomes more diffuse along H^+ (0.52), CH_3^+ (0.35), Li^+ (0.29) and Na^+ (0.26). The combined result of these two factors of HOMO–LUMO gap and overlap results in the steady decrease of the σ-orbital interactions ΔE_σ from −184.6 to −157.5 to −13.6 to −8.1 kcal mol^{-1} along CH_3^+, H^+, Li^+ and Na^+. This trend is reflected by the orbital-interaction diagram in Figure 1 which

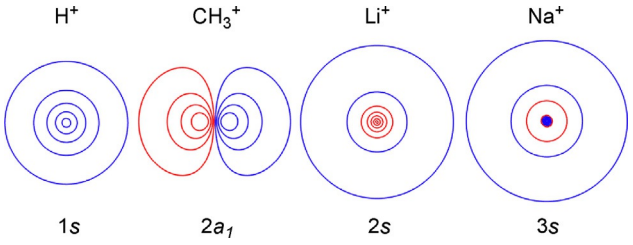

Figure 2. Contour plots of cation LUMOs (scan values: ±0.0, ±0.02, ±0.05, ±0.1, ±0.2, ±0.5).

shows that the bonding HOMO + LUMO combination in the overall complex is increasingly polarized towards the chloride fragment if one goes from $ClCH_3$ to ClH to ClLi to ClNa. In line with the trend in orbital interactions, the VDD charges of the cation-group show that the polarity of the chloride-cation bond increases if we go from hydrogen in ClH (+0.098 au) and methyl in $ClCH_3$ (+0.131 au), on one hand, to the alkali metals in ClLi and ClNa (0.475 and 0.567 au; see Table 3).

The weakening in ΔE_σ from ClLi to ClNa is reinforced by the fact that the former complex gains stabilization from the involvement of a low-lying lithium $2p_\sigma$ AO which accepts 0.08 electrons from the chloride lone pair. The corresponding sodium $3p_\sigma$ AO accepts much less, only 0.03 electrons (see Table 3; cf. 6, 36).

The π-orbital interactions ΔE_π are in all model complexes smaller than the ΔE_σ term, only slightly so for lithium and sodium cations and even significantly in the case of the proton and methyl cation. Still they follow approximately the same trend which therefore comes out even more pronouncedly in the overall orbital interactions ΔE_{oi}. The origin of the π stabilization ΔE_π is that the chloride $3p_\pi$ orbitals are stabilized in the presence of the cation. This stabilizing effect diminishes as the chloride-cation distance increases along Cl–H, Cl–Li and Cl–Na. In Cl–CH_3, these ΔE_π do not only consist of a stabilization of the chloride $3p_\pi$ orbitals in the electrostatic field of the cation but they also gain stabilization due to π-donor-acceptor interactions with the empty C–H antibonding $2e$ orbitals of CH_3^+.

Finally, the electrostatic attraction ΔV_{elstat} is in all case larger than the orbital interactions ΔE_{oi}, especially in the case of the alkali metal cation complexes. The latter have a relatively weak ΔE_{oi} term and are predominantly electrostatically bound. The relatively strong electrostatic attraction in all four model systems results from the charge separation associated with dissociation of a neutral complex into two oppositely charged fragments [Eq. (1)]. The exact trend in electrostatic attraction depends in an intricate manner on the shape and mutual penetration of the fragment charge distributions. Therefore, significant deviations of Coulombs law $q_1 \cdot q_2 / r_{12}$ for two point charges occur. Still, one can observe a slight weakening in ΔV_{elstat} from −159.9 to −159.6 to −145.1 kcal mol^{-1} as the equilibrium bond length increases along ClH to ClLi and ClNa (see Table 1 and 3).

3.3. Bonding mechanism: HCl cation affinities

The ZORA-BP86/TZ2P results of our heterolytic HCl–X^+ bonding analyses have been collected in Table 4. The cation affinity ΔH for the neutral base HCl (9 to 136 kcal mol^{-1}) are substantially smaller than those for the anionic base Cl^- (134 to 336 kcal mol^{-1}) but the trend along the four cations is the same for both bases (compare Tables 3 and 4).

The decrease in cation affinities from anionic to neutral base by 125–200 kcal mol^{-1} mainly stems from a similar weakening, that is, by 138–187 kcal mol^{-1}, in the electrostatic attraction ΔV_{elstat}. The latter is even 21 kcal mol^{-1} repulsive in the case of the proton affinity.[39] This is a direct consequence of the fact that, upon heterolytic dissociation of HCl–X^+, no charge separation occurs [Eq. (2)] while charge separation does occur for Cl–X [Eq. (1)]. Likewise, also the orbital interactions ΔE_{oi} of the neutral base HCl with the various cations (see Table 4) are weaker than the corresponding one for the anionic base (see Table 3) which has orbitals that are effectively at higher energy due to the much more negative electrostatic potential. Altogether, the weaker ΔV_{elstat} and ΔE_{oi} terms in the case of the HCl–X^+ systems lead to substantially longer Cl–X equilibrium distances (compare Tables 1 and 2) and smaller Pauli repulsion ΔE_{Pauli} (compare Tables 3 and 4). Note also the somewhat smaller deformation strain for the more weakly bound methyl cation complex $HClCH_3^+$ as compared with $ClCH_3$.

The trend in ΔE_{int} stems directly from the orbital interactions ΔE_{oi} and not from the rather weak electrostatic attraction ΔV_{elstat} anymore. The orbital interactions ΔE_{oi} become weaker from −161 to −138 to −14 to −7 kcal mol^{-1} along H^+, CH_3^+, Li^+, and Na^+. The trend in orbital interactions correlates directly with the HOMO–LUMO bond overlap (0.48, 0.32, 0.24, and 0.19) and is reflected by the population of the LUMO (0.66, 0.61, 0.05, and 0.04 e), both of which decrease along the series (see Table 4). In line with this, the polarity of the HCl–X^+ bond increases along the series, as indicated by the cation's VDD atomic charge (+0.3, +0.4, +0.7, and +0.8 a.u.).

A sizeable Pauli repulsion ΔE_{Pauli} of 103.9 kcal mol^{-1} of the HCl HOMO and HOMO^{-1} with the C–H bonding valence $1a_1$ orbital of CH_3^+ significantly weakens the MCA but does not

Table 4. Analysis of the Cl–X Bonding Mechanism between HCl and X^+.[a]

		Cation X^+			
		H^+	CH_3^+	Li^+	Na^+
Bond energy decomposition (in kcal mol^{-1})					
$\Delta E_{A'}$		−151.6	−131.3	−11.3	−5.9
$\Delta E_{A''}$		−9.4	−6.7	−2.3	−1.2
ΔE_{oi}		−161.0	−138.0	−13.7	−7.1
ΔE_{Pauli}		0.0	103.9	6.8	4.7
ΔV_{elstat}		21.0	−39.0	−8.5	−6.9
ΔE_{int}		−140.0	−73.1	−15.3	−9.4
ΔE_{strain}		0.3	15.2	0.0	0.0
ΔE_{bond}		−139.7	−57.9	−15.3	−9.4
$\Delta H_{bond} = -\Delta H_{TZ2P}$		−135.8	−54.5	−15.0	−9.3
X^+ Fragment orbital energy (in eV)					
ε_{LUMO}		−13.6	−15.1[b]	−6.9	−7.1
$\langle ClH \mid X^+ \rangle$ *Fragment orbital overlap*		$\langle 2\pi \mid 1s \rangle$	$\langle 2\pi \mid 2a_1 \rangle$	$\langle 2\pi \mid 2s \rangle$	$\langle 2\pi \mid 3s \rangle$
$\langle HOMO \mid LUMO \rangle$		0.48	0.32	0.24	0.19
Fragment orbital populations (in e)[c]					
HCl	$HOMO^{-1}$	1.95 (5σ)	1.96 (5σ)	1.98 (5σ)	1.98 (5σ)
	HOMO	1.34 (2π)	1.41 (2π)	1.87 (2π)	1.92 (2π)
X^+	LUMO	0.66 ($1s$)	0.61 ($2a_1$)	0.05 ($2s$)	0.04 ($3s$)
	LUMO + 1	0.03 ($2s$)[d]	0.00 ($3a_1$)	0.04 ($2p_\sigma$)	0.02 ($3p_\sigma$)
VDD atomic charges (in a.u.)					
Q(X in $[X–ClH]^+$)		+0.311	+0.412[e]	+0.702	+0.777

[a] Computed at ZORA-BP86/TZ2P. See also Methods section. [b] Orbital energy of CH_3^+ in the geometry it adopts in $ClCH_3$. [c] Pertinent orbital indicated in parentheses. [d] $P(2p_\sigma) = 0.03$ e. [e] Sum of atomic charges on CH_3 moiety.

change the trend.[8] Hydrogen chloride has zero Pauli repulsion with the proton (the latter has no electrons at all) and only little Pauli repulsion (4.7–6.8 kcal mol^{-1}) with the alkali metal cations which have electrons only in very compact core AOs.

4. Conclusion

Alkali metal cation affinities (AMCA) of both the anionic and neutral Lewis bases Cl^- and HCl are smaller than the corresponding proton (PA) and methyl cation affinities (MCA). Besides, all cation affinities of the neutral base HCl are weaker than those of Cl^-. This follows from our quantum chemical analyses using relativistic density functional theory.

The reason for the smaller AMCAs is mainly a weaker HOMO–LUMO interaction between the base and the alkali metal cations if compared with the proton. The AMCA therefore has a relatively large electrostatic component. The weaker HOMO–LUMO interaction originates from a higher energy (and thus a larger HOMO–LUMO gap) and more diffuse character (and thus a smaller bond overlap) of the alkali metal cation 2*s* (Li) or 3*s* (Na) LUMO. Pauli repulsion with the alkali metal cation core orbitals is relatively unimportant (although not negligible) for the weaker AMCA. At variance, Pauli repulsion is the main responsible factor for the weaker MCA as compared with PA.

The weakening of all cation affinities, if we go from anionic to the neutral base, is mainly (although not only) caused by the loss in electrostatic attraction in the latter case. In the complexes of Cl^-, there is a strong Coulomb attraction that goes with the charge separation upon heterolytic dissociation $ClX \rightarrow Cl^- + X^+$. Such charge separation does not occur for heterolytic dissociation $HClX^+ \rightarrow HCl + X^+$ in the case of the neutral base HCl.

Acknowledgements

The authors thank The Netherlands Organization for Scientific Research (NWO-CW) for financial support.

Keywords: alkali metal cation affinities · bond theory · density functional calculations · methyl cation affinities · proton affinities · thermochemistry

[1] B. L. Ellis, L. F. Nazar, *Curr. Opin. Solid State Mater. Sci.* **2012**, *16*, 168–177.
[2] T. M. Jessell, E. R. Kandel, J. H. Schwartz, *Principles of Neural Science, 4th ed.*, McGraw-Hill, New York, **2000**, pp. 154–169.
[3] B. Hille, *Ion Channels of Excitable Membranes, 3rd ed.*, Sinauer Associates, Sunderland, MA, **2001**, pp. 3–4.
[4] a) P. Li, C. Zhan, S. Zhang, X. Ding, F. Guo, S. He, J. Yao, *Tetrahedron* **2012**, *68*, 8908–8915; b) C. Hsiao, E. Tannenbaum, H. Van Deusen, E. Hershkovitz, G. Perng, A. R. Tannenbaum, L. D. Williams in *"Complexes of Nucleic Acids with Group I and II Cations" in Nucleic Acid Metal Ion Interactions* (Ed.: N. V. Hud), The Royal Society of Chemistry, London **2008**, pp. 1–35.
[5] S. Arrhenius, *Z. Phys. Chem.* **1887**, *1*, 631–648.
[6] F. M. Bickelhaupt, M. Solà, C. Fonseca Guerra, *Inorg. Chem.* **2007**, *46*, 5411–5418.
[7] a) M. Swart, F. M. Bickelhaupt, *J. Chem. Theory Comput.* **2006**, *2*, 281–287; b) M. Swart, E. Rösler, F. M. Bickelhaupt, *J. Comput. Chem.* **2006**, *27*, 1486–1493; c) M. Swart, E. Rösler, F. M. Bickelhaupt, *Eur. J. Inorg. Chem.* **2007**, 3646–3654; d) A. Moser, K. Range, D. M. York, *J. Phys. Chem. B* **2010**, *114*, 13911–13921; e) J. L. Reed, *J. Phys. Chem.* **1994**, *98*, 10477–10483; f) S. Kolboe, *J. Chem. Theory Comput.* **2014**, *10*, 3123–3128.
[8] R. J. Mulder, C. Fonseca Guerra, F. M. Bickelhaupt, *J. Phys. Chem. A* **2010**, *114*, 7604–7608.
[9] a) Computer code ADF 2013.01: E. J. Baerends, T. Ziegler, J. Autschbach, D. Bashford, A. Bérces, F. M. Bickelhaupt, C. Bo, P. M. Boerrigter, L. Cavallo, D. P. Chong, L. Deng, R. M. Dickson, D. E. Ellis, M. van Faassen, L. Fan, T. H. Fischer, C. Fonseca Guerra, M. Franchini, A. Ghysels, A. Giammona, S. J. A. van Gisbergen, A. W. Götz, J. A. Groeneveld, O. V. Gritsenko, M. Grüning, S. Gusarov, F. E. Harris, P. van den Hoek, C. R. Jacob, H. Jacobsen, L. Jensen, J. W. Kaminski, G. van Kessel, F. Kootstra, A. Kovalenko, M. V. Krykunov, E. van Lenthe, D. A. McCormack, A. Michalak, M. Mitoraj, S. M. Morton, J. Neugebauer, V. P. Nicu, L. Noodleman, V. P. Osinga, S. Patchkovskii, M. Pavanello, P. H. T. Philipsen, D. Post, C. C. Pye, W. Ravenek, J. I. Rodriguez, P. Ros, P. R. T. Schipper, H. van Schoot, G. Schreckenbach, J. S. Seldenthuis, M. Seth, J. G. Snijders, M. Solà, M. Swart, D. Swerhone, G. te Velde, P. Vernooijs, L. Versluis, L. Visscher, O. Visser, F. Wang, T. A. Wesolowski, E. M. van Wezenbeek, G. Wiesenekker, S. K. Wolff, T. K. Woo, A. L. Yakovlev, Scientific Computing and Modeling (SCM), Theoretical Chemistry, VU University Amsterdam, Amsterdam (The Netherlands), **2013**; b) http://www.scm.com.
[10] G. te Velde, F. M. Bickelhaupt, E. J. Baerends, C. Fonseca Guerra, S. J. A. van Gisbergen, J. G. Snijders, T. Ziegler, *J. Comput. Chem.* **2001**, *22*, 931–967.
[11] E. van Lenthe, E. J. Baerends, *J. Comput. Chem.* **2003**, *24*, 1142–1156.
[12] J. C. Slater, *Phys. Rev.* **1951**, *81*, 385–390.
[13] S. H. Vosko, L. Wilk, M. Nusair, *Can. J. Phys.* **1980**, *58*, 1200–1211.
[14] J. P. Perdew, *Phys. Rev. B* **1986**, *33*, 8822–8824; Erratum: J. P. Perdew, *Phys. Rev. B* **1986**, *34*, 7406.
[15] A. D. Becke, *Phys. Rev. A* **1988**, *38*, 3098–3100.
[16] M. Swart, J. G. Snijders, *Theor. Chem. Acc.* **2003**, *110*, 34–41; Erratum: M. Swart, J. G. Snijders, *Theor. Chem. Acc.* **2004**, *111*, 56.
[17] E. van Lenthe, E. J. Baerends, J. G. Snijders, *J. Chem. Phys.* **1993**, *99*, 4597–4610.
[18] a) A. D. Becke, *J. Chem. Phys.* **1993**, *98*, 5648–5652; b) P. J. Stephens, F. J. Devlin, C. F. Chabalowski, M. J. Frisch, *J. Phys. Chem.* **1994**, *98*, 11623–11627.
[19] a) P. Atkins, J. de Paula, *Atkins' Physical Chemistry*, Oxford University Press, Oxford, **2002**; b) F. Jensen, *Introduction to Computational Chemistry, 2nd ed.*, Wiley & Sons, Chichester, West Sussex, **2007**.
[20] a) F. M. Bickelhaupt, E. J. Baerends in *Reviews in Computational Chemistry, Vol. 15* (Eds.: K. B. Lipkowitz, D. B. Boyd), Wiley-VCH, Weinheim, **2000**, pp. 1–86; b) T. Ziegler, A. Rauk, *Theor. Chim. Acta.* **1977**, *46*, 1–10; c) T. Ziegler, A. Rauk, *Inorg. Chem.* **1979**, *18*, 1558–1565; d) T. Ziegler, A. Rauk, *Inorg. Chem.* **1979**, *18*, 1755–1759.
[21] F. M. Bickelhaupt, N. J. R. van Eikema Hommes, C. Fonseca Guerra, E. J. Baerends, *Organometallics* **1996**, *15*, 2923–2931.
[22] See also: a) C. Fonseca Guerra, F. M. Bickelhaupt, J. G. Snijders, E. J. Baerends, *Chem. Eur. J.* **1999**, *5*, 3581–3594; b) C. Fonseca Guerra, J. W. Handgraaf, E. J. Baerends, F. M. Bickelhaupt, *J. Comput. Chem.* **2004**, *25*, 189–210; Voronoi cells are equivalent to Wigner–Seitz cells in crystals; for the latter, see: c) C. Kittel, *Introduction to Solid State Physics*, Wiley, New York, **1986**.
[23] G. te Velde, E. J. Baerends, *J. Comput. Phys.* **1992**, *99*, 84–98.
[24] C. K. Kim, J. Won, H. S. Kim, Y. S. Kang, H. G. Li, C. K. Kim, *J. Comput. Chem.* **2001**, *22*, 827–834.
[25] K. E. Gutowski, J. D. Holbrey, R. D. Rogers, D. A. Dixon, *J. Phys. Chem. B* **2005**, *109*, 23196–23208.
[26] C. Mayeux, P. Burk, *J. Phys. Chem. A* **2014**, *118*, 1906–1917.
[27] E. Uggerud, *Eur. J. Mass Spectrom.* **2000**, *6*, 131–134.
[28] *NIST Chemistry WebBook, NIST Standard Reference Database Number 69* (Eds.: P. J. Linstrom, W. G. Mallard), National Institute of Standards and Technology, Gaithersburg, MD, http://webbook.nist.gov, retrieved December 19, **2014**.
[29] A. L. L. East, B. J. Smith, L. Radom, *J. Am. Chem. Soc.* **1997**, *119*, 9014–9020.

[30] Y. Wei, T. Singer, G. N. Sastry, H. Zipse, *J. Comput. Chem.* **2008**, *29*, 291 – 297.
[31] J. Del Bene, *J. Phys. Chem.* **1996**, *100*, 6284 – 6287.
[32] T. McMahon, T. Heinis, G. Nicol, J. K. Hovey, P. Kebarle, *J. Am. Chem. Soc.* **1988**, *110*, 7591 – 7598.
[33] R. A. Perry, B. R. Rowe, A. A. Viggiano, D. L. Albritton, E. E. Ferguson, F. C. Fehsenfeld, *Geophys. Res. Lett.* **1980**, *7*, 693 – 696.
[34] a) F. M. Bickelhaupt, R. L. DeKock, E. J. Baerends, *J. Am. Chem. Soc.* **2002**, *124*, 1500 – 1505; b) F. M. Bickelhaupt, E. J. Baerends, *Angew. Chem. Int. Ed.* **2003**, *42*, 4183 – 4188; *Angew. Chem.* **2003**, *115*, 4315 – 4320.
[35] F. M. Bickelhaupt, M. Solà, C. Fonseca Guerra, *J. Comput. Chem.* **2007**, *28*, 238 – 250.
[36] F. M. Bickelhaupt, M. Solà, C. Fonseca Guerra, *J. Chem. Theory Comput.* **2006**, *2*, 965 – 980.
[37] F. M. Bickelhaupt, T. Ziegler, P. v. R. Schleyer, *Organometallics* **1996**, *15*, 1477 – 1487.
[38] a) J. M. Ruiz, R. J. Mulder, C. Fonseca Guerra, F. M. Bickelhaupt, *J. Comput. Chem.* **2011**, *32*, 681 – 688; b) J. M. Ruiz, C. Fonseca Guerra, F. M. Bickelhaupt, *J. Phys. Chem. A* **2011**, *115*, 8310 – 8315.
[39] If one elongates the HCl–H^+ bond beyond its equilibrium value, ΔV_{elstat} becomes stabilizing again.

Received: November 15, 2015
Revised: January 26, 2016
Published online on February 22, 2016

